Impedance Measurement of Wind Turbines Using a Multimegawatt Grid Simulator

Preprint

Shahil Shah, Przemyslaw Koralewicz, Vahan Gevorgian, and Robb Wallen

National Renewable Energy Laboratory

Presented at the 18th Wind Integration Workshop
Dublin, Ireland
October 16-18, 2019

NREL is a national laboratory of the U.S. Department of Energy
Office of Energy Efficiency & Renewable Energy
Operated by the Alliance for Sustainable Energy, LLC

This report is available at no cost from the National Renewable Energy Laboratory (NREL) at www.nrel.gov/publications.

Contract No. DE-AC36-08GO28308

Conference Paper
NREL/CP-5D00-74890
November 2019

Impedance Measurement of Wind Turbines Using a Multimegawatt Grid Simulator

Preprint

Shahil Shah, Przemyslaw Koralewicz, Vahan Gevorgian, and Robb Wallen

National Renewable Energy Laboratory

Suggested Citation
Shah, Shahil, Przemyslaw Koralewicz, Vahan Gevorgian, and Robb Wallen. 2019. *Impedance Measurement of Wind Turbines Using a Multimegawatt Grid Simulator: Preprint*. Golden, CO: National Renewable Energy Laboratory. NREL/CP-5D00-74890. https://www.nrel.gov/docs/fy20osti/74890.pdf.

NREL is a national laboratory of the U.S. Department of Energy
Office of Energy Efficiency & Renewable Energy
Operated by the Alliance for Sustainable Energy, LLC

This report is available at no cost from the National Renewable Energy Laboratory (NREL) at www.nrel.gov/publications.

Contract No. DE-AC36-08GO28308

Conference Paper
NREL/CP-5D00-74890
November 2019

National Renewable Energy Laboratory
15013 Denver West Parkway
Golden, CO 80401
303-275-3000 • www.nrel.gov

NOTICE

This work was authored by the National Renewable Energy Laboratory, operated by Alliance for Sustainable Energy, LLC, for the U.S. Department of Energy (DOE) under Contract No. DE-AC36-08GO28308. Funding provided by U.S. Department of Energy Office of Energy Efficiency and Renewable Energy Wind Energy Technologies Office. The views expressed herein do not necessarily represent the views of the DOE or the U.S. Government. The U.S. Government retains and the publisher, by accepting the article for publication, acknowledges that the U.S. Government retains a nonexclusive, paid-up, irrevocable, worldwide license to publish or reproduce the published form of this work, or allow others to do so, for U.S. Government purposes.

Cover Photos by Dennis Schroeder: (clockwise, left to right) NREL 51934, NREL 45897, NREL 42160, NREL 45891, NREL 48097, NREL 46526.

Impedance Measurement of Wind Turbines using a Multimegawatt Grid Simulator

Shahil Shah, Przemyslaw Koralewicz, Vahan Gevorgian, and Robb Wallen

National Renewable Energy Laboratory (NREL), Golden, CO 80401, USA
Email: {Shahil.Shah, Przemyslaw.Koralewicz, Vahan.Gevorgian, Robb.Wallen}@nrel.gov

***Abstract*–This paper presents the impedance measurements of a 4 MW wind turbine conducted using a multimegawatt grid simulator at the National Renewable Energy Laboratory in Colorado, United States. This paper describes different systems, including a 7 MVA grid simulator, a 5 MW dynamometer, a medium-voltage measurement system, and a real-time control system used for the automated impedance measurement of a utility-scale wind turbine. Different aspects of impedance measurement are discussed, including the selection of the magnitude of injected perturbation, measurement of frequency cross-coupling between the sequence impedance responses, and the alignment of the reference frame for sequence impedance measurement. The paper also demonstrates high-fidelity validation of an EMT simulation model of the wind turbine using impedance measurements.**

I. Introduction

Impedance-based stability analysis has proven effective for the evaluation and mitigation of control interactions in land-based and offshore wind power plants, including subsynchronous and super-synchronous resonance conditions as well as interactions with the HVDC link [1]–[3]. Transmission system operators (TSOs) have started demanding that manufacturers provide the impedance response data of wind turbines to support the thorough evaluation of the stability impacts of wind power plants. Impedance-based specifications for wind turbines are also being developed to reduce the risks of resonance problems. These developments in the wake of increasing number of stability events involving wind power plants have made the impedance measurement of wind turbines an important grid integration test.

The impedance response of a wind turbine can be measured by injecting voltage or current perturbations at different frequencies from its terminals superimposed on the steady-state voltages and currents at the fundamental frequency [4]. Impedance characterization of a wind turbine using controller-hardware-in-the-loop (CHIL) simulations using only the wind turbine controller is also possible [5], [6]; however, direct impedance measurement is crucial for checking compliance of a wind turbine with the emerging impedance-based grid codes. Additionally, the accuracy of the CHIL-simulation-based impedance characterization is highly dependent on the accuracy of the simulated power hardware models. Moreover, establishing the interface between the turbine controller and the digital simulator for each turbine for impedance characterization can be a major challenge.

Multimegawatt grid simulators have been used to test wind turbine generators during transient events[†]. Tests conducted at utility-scale grid-simulator facilities include: i) fault ride-through tests; ii) testing of volt-VAR and frequency-watt characteristics, iii) anti-islanding tests, iv) harmonic emission tests, and v) testing of operation with specific grid impedance. This paper presents the impedance measurement of a 4 MW wind turbine using a multimegawatt grid simulator test bed at the National Renewable Energy Laboratory (NREL) in Colorado, United States. This paper describes the test bed components used for the impedance measurement. It also discusses the measurement of the coupling between the positive- and negative-sequence impedance responses and the alignment of the reference frame for the sequence impedance measurement. The paper shows that similar to the dq impedance responses, the sequence impedance responses are also attached to a reference frame. The paper also shows high-fidelity validation of an EMT simulation model of the wind turbine using impedance measurements.

The rest of the paper is organized as follows: Section II describes the grid simulator test bed at NREL, Section III presents the impedance measurements of a 4 MW Type-III wind turbine drivetrain and discusses different aspects of impedance characterization, Section IV presents impedance-based validation of EMT simulation models, and Section V concludes this paper.

II. Impedance Measurement Testbed

The multimegawatt grid simulator is the key technology for testing utility-scale wind turbines under different grid conditions. One such grid simulator, called the controllable grid interface (CGI), was commissioned at NREL in 2013–2014 [8]. The CGI

This work was authored by Alliance for Sustainable Energy, LLC, the manager and operator of the National Renewable Energy Laboratory for the U.S. Department of Energy (DOE) under Contract No. DE-AC36-08GO28308. Funding provided by U.S. Department of Energy Office of Energy Efficiency and Renewable Energy Wind Energy Technologies Office. The views expressed in the article do not necessarily represent the views of the DOE or the U.S. Government. The U.S. Government retains and the publisher, by accepting the article for publication, acknowledges that the U.S. Government retains a nonexclusive, paid-up, irrevocable, worldwide license to publish or reproduce the published form of this work, or allow others to do so, for U.S. Government purposes.

[†]*Proc. 2018 Annual Int. Workshop on Grid Simulator Testing*, Tallahassee, FL, USA provides an excellent overview of utility-scale grid simulator facilities around the world and electrical characterization tests performed at these facilities on wind turbine generators, PV inverters, and energy storage systems [7].

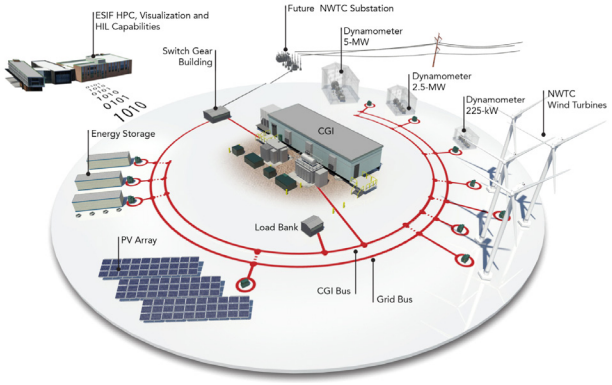

Fig. 1. Infrastructure at NREL centered around a multimegawatt grid simulator for grid integration research and testing. Illustration by Josh Bauer, NREL.

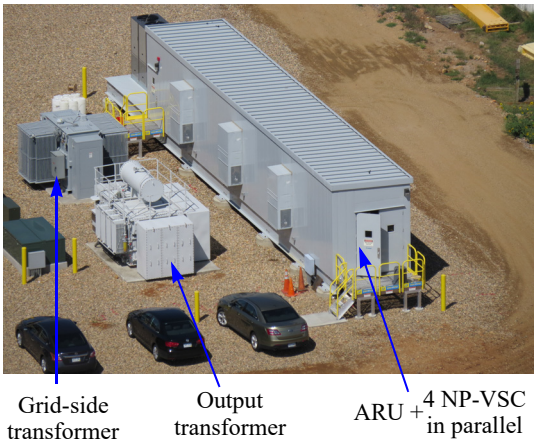

Fig. 2. 13.8 kV, 7 MVA grid simulator called controllable grid interface (CGI) custom designed using ABB's medium voltage ACS6000 drive technology. Source: Mark McDade, NREL.

is the centerpiece of a grid integration testbed at NREL, which also includes several utility-scale wind turbines, PV arrays, battery energy storage systems, multimegawatt dynamometers for testing wind turbine nacelles, a medium-voltage data acquisition system (MVDAS), and digital simulation platforms enabling power-hardware-in-the-loop (PHIL) and CHIL simulations. Fig. 1 shows an illustration of the grid integration testbed. The following subsections discuss components of the testbed used for the impedance measurement of wind turbines.

A. Grid Simulator

The CGI at NREL is shown in Fig. 2; it is rated for 13.8 kV, 7 MVA continuous power, and 39 MVA short-term rating for 2 seconds. It is custom designed based on ABB's ACS6000 industrial-grade medium-voltage drive technology. It features a 9 MVA active rectifier unit (ARU) at the utility side that regulates the intermediate dc bus voltage. The controllable grid is established by four front-end neutral-point-clamped inverters, each with the rated output of 3.3 kV, connected in parallel. A specialized multi-winding output transformer shown in Fig. 2 is

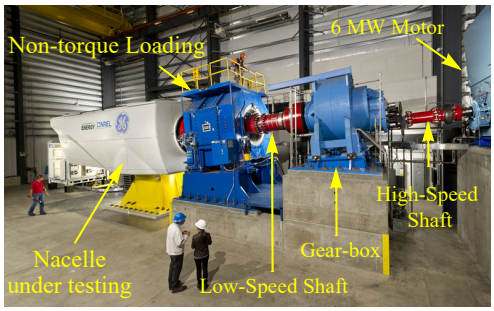

Fig. 3. 5 MW dynamometer for wind turbine nacelle testing. Source: Dennis Schroeder, NREL.

used to synthesize 17-level low-distortion voltage waveforms by combining 3-level phase voltages from the inverters. The transformer also steps up the voltage to 13.8 kV. The CGI is designed to simultaneously meet the following requirements: multimegawatt power rating, sub-1% THD in the voltage waveforms, and an extremely fast response time of less than 1 ms. The fast dynamics of the CGI enable it to behave like an ideal voltage source that can be configured for injecting voltage perturbations over a broad frequency range for impedance measurements.

B. Dynamometer

Impedance measurement of wind turbine nacelles for specific operation conditions, including active and reactive power output and rotating speed, requires a mechanical prime mover that can emulate the behavior of the wind turbine rotor for different wind conditions. A 5 MW dynamometer shown in Fig. 3 is used for this purpose in the grid integration testbed at NREL [9].

C. GPS-Synchronized Medium-Voltage Measurements

The testbed has an MVDAS, which is a distributed network of GPS-synchronized measurement nodes sampling three-phase voltage and current waveforms at 50 kHz with 24 bit resolution. Raw 50 kHz voltage and current waveform captures can be triggered by programmable thresholds, supervisory control, or asynchronously by an user interface and stored locally for post-event downloading, alignment, and processing. Fig. 4 shows hardware inside the sensor nodes, including capacitive voltage sensors [10], rogowski-coil-based current sensors [11], and a GPS-synchronized signal conditioning unit built around NI 9030 cRIO platform. MVDAS nodes are located at different points in the testbed shown in Fig. 1, and they allow for the GPS-synchronized measurement of voltages and currents during the injection of sinusoidal perturbations to obtain an impedance response over a broad frequency range.

D. Real-Time Control System

To enable the impedance measurement, all the components described above are integrated as shown in Fig. 5. The CGI is controlled by an RTDS system using a fast 2 Gbit/s optical fiber interface [12]. The CGI control system is tested for the injection of perturbations over a wide spectrum of frequencies from 0.1 Hz to 3 kHz. As shown in Fig. 6, the control system synthesizes

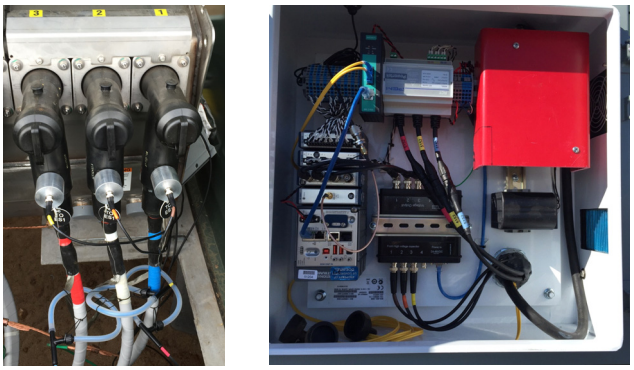

a) b)

Fig. 4. Hardware in each MVDAS sensing node: a) voltage and current sensors; b) data conditioning built around NI 9030 cRIO platform. Source: NREL.

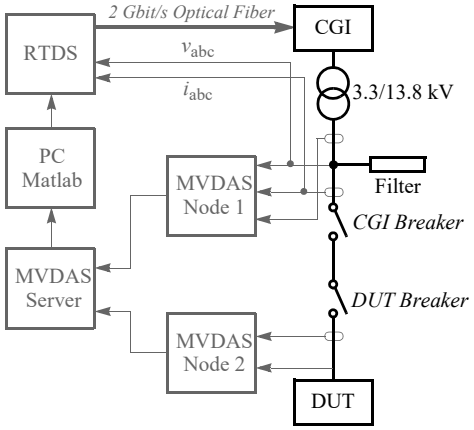

Fig. 5. Impedance measurement system diagram.

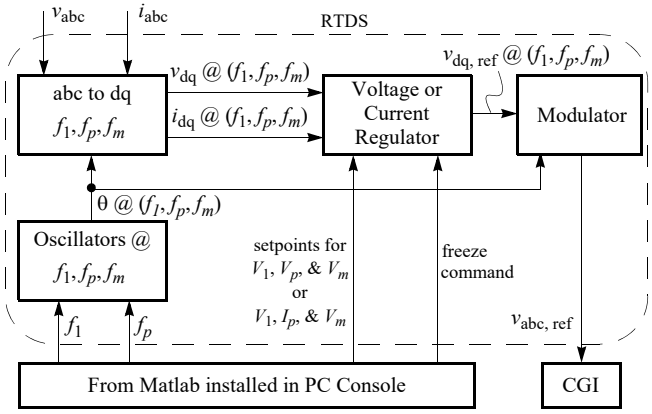

Fig. 6. Control of fundamental, perturbation, and mirror frequency components.

voltage references for the CGI, which consist of components at the fundamental frequency, f_1, perturbation frequency, f_p, and mirror frequency, $f_m = f_p - 2 \cdot f_1$ [2]. The magnitude of the mirror frequency component is regulated at zero for the accurate measurement of the impedance response [2].

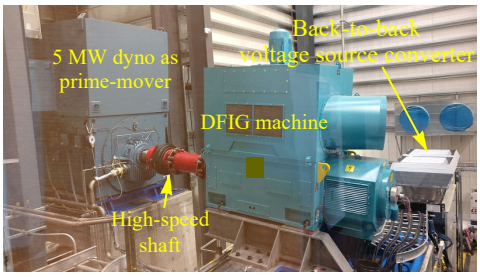

Fig. 7. Type III wind turbine drivetrain of around 4 MW rating. Source: NREL.

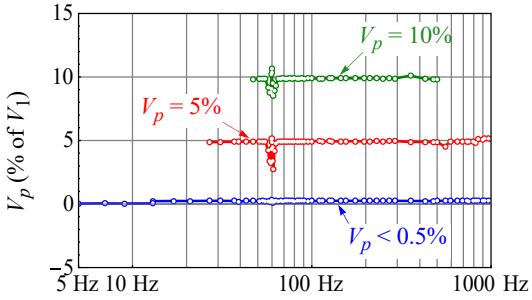

Fig. 8. Magnitude of the injected positive-sequence voltage perturbation, V_p, injected for three impedance measurement sweeps of a 4 MW wind turbine.

III. Impedance Measurement

A. Sequence Impedance Measurement

Fig. 7 shows a 4 MW Type III wind turbine drivetrain, including a doubly-fed induction generator (DFIG) and back-to-back voltage source converters whose sequence impedance responses are measured using the impedance measurement system described in the previous section. The 4 MW DFIG is driven at a constant speed using the 5 MW dynamometer to test its behavior for different wind speeds, particularly for operation at subsynchronous and super-synchronous rotating speeds.

For the positive-sequence impedance measurement, the CGI injects positive-sequence voltage perturbations superimposed on the nominal fundamental trajectory. Fig. 8 shows the voltage perturbation magnitude, V_p, during three impedance sweeps of the DFIG, demonstrating that the perturbation magnitude is actively regulated during each impedance sweep. Note that V_p in Fig. 8 is represented in terms of the percentage of the nominal peak phase voltage, V_1; hence, the magnitude of the injected voltage perturbation in each phase is 1,127 V ($=0.1 \cdot \sqrt{2/3} \cdot 13.8\text{x}10^3$) for the 10% perturbation condition. Voltage and current waveforms at the turbine terminals for a specific perturbation point (f_p = 477 Hz; V_p = 10%) are shown in Fig. 9. Fig. 10 shows measured positive-sequence impedance responses of the 4 MW DFIG drivetrain for different perturbation magnitudes. The accuracy of the impedance measurement system is verified by comparing the measured impedance response of a three-phase filter connected at the CGI terminals with the analytical prediction using the filter parameters.

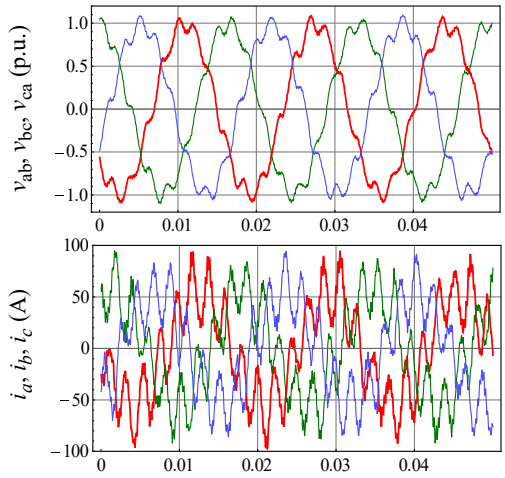

Fig. 9. Line-to-line voltages and output currents of the 4 MW turbine drivetrain during injection of 10% positive-sequence voltage perturbation at 477 Hz.

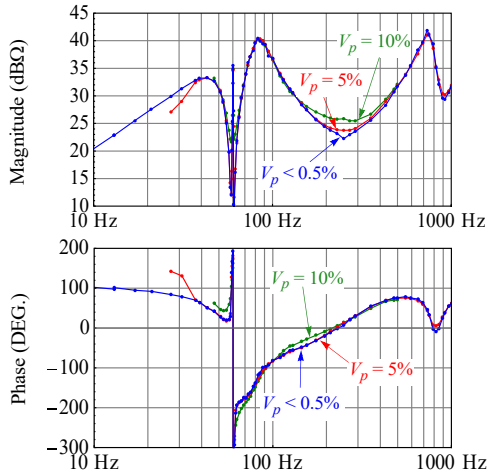

Fig. 10. Positive-sequence impedance response of a 4 MW DFIG-based wind turbine drivetrain for different magnitudes of the injected voltage perturbation.

B. Reference Frame of Sequence Impedance

As shown in [2], because of the time-periodic nature of their dynamics, three-phase power electronics devices such as wind turbines, inverters, etc., usually exhibit a frequency cross-coupled response: the injection of a positive-sequence voltage perturbation at frequency f_p produces a positive-sequence response at frequency f_p as well as a negative-sequence response at frequency f_p–$2f_1$; the latter can also be interpreted as positive-sequence response at frequency $2f_1$–f_p. A similar cross-coupled response is also present for the injection of negative-sequence perturbations. Stability analysis at frequencies closer to the fundamental frequency must account for these coupling effects [2]. This coupling between the positive and negative sequence dynamics can be accounted for by a sequence admittance matrix [2]:

$$\begin{bmatrix} I_p(s+j\omega_1) \\ I_n(s-j\omega_1) \end{bmatrix} = \begin{bmatrix} Y_{pp}(s) & Y_{pn}(s) \\ Y_{np}(s) & Y_{nn}(s) \end{bmatrix} \begin{bmatrix} V_p(s+j\omega_1) \\ V_n(s-j\omega_1) \end{bmatrix} \quad (1)$$

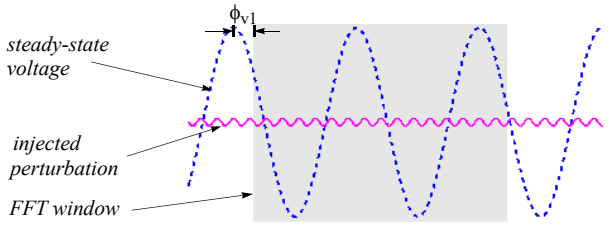

Fig. 11. Reference frame of sequence-domain impedance response.

where $s = j2\pi f_p$, and subscripts p and n, respectively, denote the positive- and negative-sequence components of the three-phase voltages and currents at the terminals of the equipment.

The elements of the admittance matrix are related, and the terminal behavior of a turbine can be completely described in the sequence-domain using the following two transfer functions [2]:

$$Y_p(s) = \frac{I_p(s)}{V_p(s)} \text{ and } Y_c(s) = \frac{I_n(s-j2\omega_1)}{V_p(s)} \quad (2)$$

where $Y_p(s)$ and $Y_c(s)$, respectively, represent the positive-sequence direct admittance and coupling admittance. The coupling admittance, $Y_c(s)$, can be measured by extracting the negative-sequence response in the output currents of the device at frequency f_p–$2f_1$ when a positive-sequence voltage perturbation is injected at frequency f_p.

The phase response of the coupling admittance, $Y_c(s)$, [as well as of $Y_{pn}(s)$ and $Y_{np}(s)$] for each perturbation frequency is dependent on the starting point of the data window used for the FFT analysis. In other words, the phase response of $Y_c(s)$ is dependent on angle ϕ_{v1} defined in Fig. 11. Because ϕ_{v1} is time-periodic in nature, the phase response of $Y_c(s)$ is also time-periodic; this is because of the time-periodic nature of the dynamics of power electronic devices connected to an ac network. The coupling admittance must be measured for the same value of ϕ_{v1} for each perturbation frequency; this requires synchronization of the FFT window with a specific point on the fundamental trajectory of the voltages at the turbine terminals. Synchronization of data captures is difficult; instead, a method is presented here to compensate the non-synchronized data captures during post-processing of the measurements.

In this paper, ϕ_{v1}=0 is used as the reference frame for the sequence impedance measurement. This is equivalent to aligning the d-axis for the dq impedance measurement with the phase a voltage. It can be shown that if,

$$\angle Y_c(s)\big|_{\phi_{v1}=0} = \Theta \quad (3)$$

then,

$$\angle Y_c(s)\big|_{\phi_{v1}=\alpha} = \Theta - 2\alpha \quad (4)$$

The factor 2α in (4) is the result of the mismatch of $2\omega_1$ in the frequencies of the voltage and current perturbations in the definition of $Y_c(s)$ in (2). Comparing (3) and (4), we get:

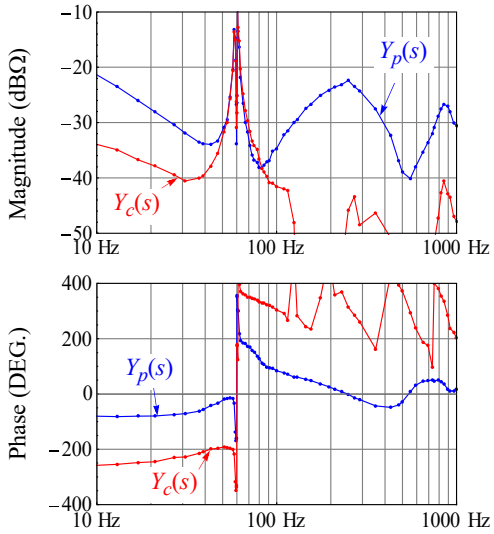

Fig. 12. Frequency cross-coupling between the positive and negative sequence admittance responses of the 4 MW Type III wind turbine drivetrain. Blue lines: response of the positive-sequence direct admittance $Y_p(s)$ and red lines: response of the positive-sequence coupling admittance $Y_c(s)$.

$$\angle Y_c(s)\big|_{\phi_{v1}=0} = \angle Y_c(s)\big|_{\phi_{v1}=\alpha} + 2\alpha \qquad (5)$$

Eq. (5) can be used to obtain the phase-response of $Y_c(s)$ in the reference frame defined by ϕ_{v1}=0 by using the phase angle of the fundamental component of the voltages at the turbine terminals, which is obtained by FFT analysis.

Fig. 12 compares the measured responses of $Y_p(s)$ and $Y_c(s)$ of the 4 MW DFIG obtained by following the above described alignment process. Clearly, the coupling admittance, $Y_c(s)$, is as significant as the direct admittance, $Y_p(s)$, around the fundamental frequency. This proves experimentally that the evaluation of resonance in wind power plants near the fundamental frequency (<200 Hz) must consider the frequency cross-coupling between the positive- and negative-sequence impedance responses of the wind turbines [2]. Note that $Y_c(s)$ is significantly smaller than $Y_p(s)$ away from the fundamental frequency, implying that the cross-coupling is much smaller and can be ignored for the evaluation of resonance conditions away from the fundamental frequency [2]. Another inference from the above discussion is that similar to the dq impedance responses, sequence impedance responses also have a reference frame defined by the starting point of the FFT window with respect to the phase of the terminal voltages at the fundamental frequency.

The non-negligible internal impedance of the CGI may result in a negative-sequence voltage perturbation at the mirror frequency $f_m = f_p - 2f_1$ because of the coupling current response at this frequency. This may introduce errors in the impedance measurements. This is avoided by actively regulating the negative-sequence voltage component at the mirror frequency f_m to zero using the CGI control system shown in Fig. 6. The performance of the control system in eliminating the voltage perturbation component at frequency f_m is shown in Fig. 13.

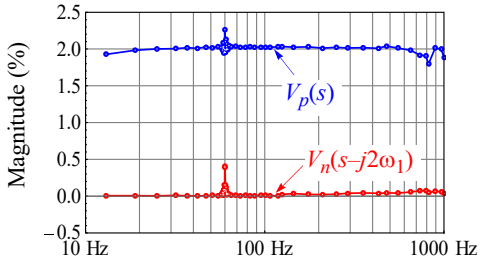

Fig. 13. Active regulation of the magnitudes of the injected positive-sequence voltage perturbation $V_p(s)$ and the mirror negative-sequence voltage perturbation $V_n(s-j2\omega_1)$. In this case $V_p(s)$ is regulated at 2% and $V_n(s-j2\omega_1)$ is regulated at 0% to avoid measurement errors because of frequency cross-coupling effects.

C. *Magnitude of Injected Perturbation*

Small-signal impedance measurements are performed by injecting perturbations with magnitudes as small as possible. Small-signal impedance-based stability analysis is effective for the evaluation of control interaction and resonance problems [1]; however, small-signal impedance analysis cannot predict the magnitude of resonance, i.e. the amplitude of the resonance-generated oscillations, which is important for the protection and control design of wind turbines as well as for the estimation of power quality during different operation conditions. As shown in [13], nonlinearities change the impedance response of wind turbines, inverters, HVDC converters, etc., as the perturbation magnitude is increased. The set of impedance responses for different perturbation magnitudes, which is referred to as large-signal impedance in [13], [14], can be used to predict the magnitude of oscillations during resonance events. As demonstrated in Fig. 10, the CGI-based impedance measurement system can actively regulate the magnitude of the injected perturbation, enabling both small-signal and large-signal impedance measurement of wind turbines.

Impedance sweeps of the 4 MW wind turbine drivetrain are performed by gradually increasing the injected perturbation magnitude until the turbine starts tripping because of the overcurrent protection. Such a set of impedance responses not only predicts the magnitude of the resonance-generated oscillations the turbine will experience under different grid conditions but also characterizes the response of its protection systems to oscillations at non-fundamental frequencies. Fig. 8 shows that the range of impedance sweeps of the 4 MW turbine starts narrowing as the injected perturbation magnitude is increased. This is because the turbine starts tripping for the higher perturbation magnitudes, particularly when the perturbation frequency is away from the fundamental frequency. Hence, the large-signal impedance responses also show the range of resonance magnitudes and frequencies that are not sustainable by a wind turbine; the turbine will trip if any negatively damped resonance condition pushes it in the zone where the resonance is not sustainable.

It is worth noting here that in addition to the changing impedance response of wind turbines with the resonance magnitude, the changing impedance response of the transmission

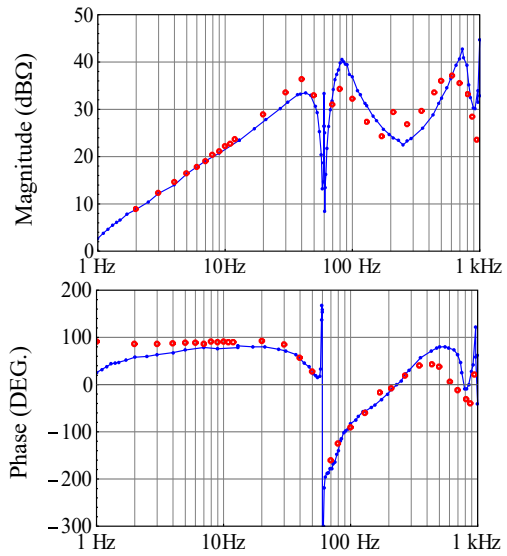

Fig. 14. Positive-sequence impedance response of the 4 MW Type III wind turbine drivetrain obtained by measurements using CGI (blue solid lines) and using simulations of a PSCAD model from the turbine manufacturer (red points).

network with the resonance magnitude also determines the magnitude of the resonance-generated oscillations; for instance, the magnitude of subsynchronous resonance (SSR) in Type III wind power plants in proximity of series compensated transmission lines is predominantly governed by the change in the transmission network impedance during resonance because of the surge protection of the series compensation capacitors [3].

IV. EMT Model Validation

Turbine manufactures validate the EMT simulation models of wind turbines for control design and grid impact studies by comparing the model response with the turbine response to a transient test conducted at a grid-simulator facility [7]. The time-domain transient tests using a grid-simulator do not excite the entire dynamic space of the device, making the model validation questionable. Impedance response characterizes the turbine behavior at discrete frequency points over a broad frequency range. Hence, it can efficiently serve as a model validation tool. Fig. 14 compares the positive-sequence impedance response measurement of the 4 MW Type-III wind turbine drivetrain shown in Fig. 7c) with that obtained using a PSCAD model developed by the manufacture. The impedance response from the PSCAD model matches closely with the measured response, verifying the accuracy of the simulation model. Impedance-validated simulation models can be used to carry out large-scale grid-integration studies, including transient studies such as evaluation of the fault ride-through performance as well as dynamic studies for the evaluation of stability and resonance problems.

V. Conclusion

This paper presented impedance measurement of a utility-scale wind turbine using a multimegawatt grid simulator testbed. Different aspects of sequence impedance measurement including the selection of the perturbation magnitude, measurement of the frequency cross-coupling between the positive and negative sequence impedance responses, and the alignment of the reference frame for sequence impedance measurement are discussed. The paper showed that the sequence impedance responses of wind turbines are aligned with a reference frame similar to the dq impedance responses. The paper also demonstrated high-fidelity validation of an EMT simulation model of the wind turbine using impedance measurements. Impedance measurement of wind turbines using multimegawatt grid simulators as presented in this paper will play an important role in the future as new grid codes emerge for wind turbines based on the impedance response specifications to mitigate the risks of dynamics stability and resonance problems.

References

[1] J. Sun, M. Li, Z. Zhang, T. Xu, J. He, H. Wang, and G. Li, "Renewable energy transmission by HVDC across the continent: system challenges and opportunities," *CSEE J. Power and Energy Syst.*, vol. 3, no. 4, pp. 353-364, Dec. 2017.

[2] S. Shah and L. Parsa, "Impedance modeling of three-phase voltage source converters in DQ, sequence, and phasor domains," *IEEE Trans. Energy Conv.*, vol. 32, no. 3, pp. 1139-1150, April 2017.

[3] S. Shah, V. Gevorgian, and H. Liu, "Impedance-based prediction of SSR-generated harmonics in doubly-fed induction generators," in *Proc. 2019 IEEE Power Energy Soc. Gen. Meet. (PESGM)*, Atlanta, GA.

[4] S. Shah, P. Koralewicz, R. Wallen, and V. Gevorgian, "Impedance characterization of utility-scale renewable energy and storage systems," in *Proc. 2019 Energy Conv. Cong. Expo. (ECCE)*, Baltimore, MD.

[5] S. Shah, I. Vieto, and J. Sun, "Real-time simulation of wind turbine converter-grid systems," in *Proc. 2014 Int. Power Electron. Conf. (IPEC)*, Hiroshima, Japan.

[6] G. Li and J. Sun, "Control hardware-in-the-loop simulation for turbine impedance modeling and verification," in *Proc. of the 16th Wind Integration Workshop*, Berlin, 2017.

[7] *Fifth Int. Workshop on Grid Simulator Testing of Wind Turbine Powertrains*, Tallaahasse, FL, USA, Nov. 2018. [Online] Available: https://www.nrel.gov/grid/workshop-grid-simulator-2018-proceedings.html

[8] P. Koralewicz et. al., "Advanced grid simulator for multi-megawatt power converter testing and certification," in *Proc. 2016 IEEE Energy Conv. Cong. Expo. (ECCE)*, 2016, Milwaukee, WI, USA.

[9] S. Lambert, V. Gevorgian, S. Dana, and R. Wallen, "Phase 1 integrated systems test and characterization report for the 5-Megawatt dynamometer and controllable grid interface," NREL, Golden, CO, USA, Tech. Rep. NREL/TP-5000-63073, Mar. 2018.

[10] Jomitek – Powerful Solutions, "The Jomitek v3 voltage sensor," Datasheet, 2012.

[11] Powertek - RCTi current sensors, "RCTi single-phase current transducer," Datasheet. [Online] www.powertekuk.com/rcti-single-phase-current-transducer.pdf, accessed on July 17, 2019.

[12] P. Koralewicz, V. Gevorgian, and R. Wallen, "Multimegawatt-scale power hardware-in-the-loop interface for testing ancillary grid services by converter coupled generations," in *Proc. 2017 IEEE 18th Workshop on Control and Modeling for Power Electron. (COMPEL)*, Stanford, CA.

[13] S. Shah and L. Parsa, "Impedance-based prediction of distortions generated by resonance in grid-connected converters," *IEEE Trans. Energy Conv.*, Mar. 2019. doi: 10.1109/TEC.2019.2904674

[14] S. Shah, et. al., "Large-signal impedance-based modeling and mitigation of resonance of converter-grid systems," *IEEE Trans. Sustain. Energy*, vol. 10, no. 3, pp. 1439-1449, July 2019.